

High Order Residual Distribution Conservative Finite Difference HWENO Scheme for Steady State Problems

Jianfang Lin ¹, Yupeng Ren ², Rémi Abgrall ³, Jianxian Qiu⁴

Abstract. In this paper, we develop a high order residual distribution (RD) method for solving steady state conservation laws in a novel Hermite weighted essentially non-oscillatory (HWENO) framework recently developed in [23]. In particular, we design a high order HWENO reconstructions for the integrals of source term and fluxes based on the point values of the solution and its spatial derivatives, and the principles of residual distribution schemes are adapted to obtain steady state solutions. The proposed novel HWENO framework enjoys two advantages. First, compared with the traditional HWENO framework, the proposed methods do not need to introduce additional auxiliary equations to update the derivatives of the unknown function, and compute them from the current value and the old spatial derivatives. This approach saves the computational storage and CPU time, which greatly improves the computational efficiency of the traditional HWENO framework. Second, compared with the traditional WENO method, reconstruction stencil of the HWENO methods becomes more compact, their boundary treatment is simpler, and the numerical errors are smaller at the same grid. Thus, it is also a compact scheme when we design the higher order accuracy, compared with that in [11] Chou and Shu proposed. Extensive numerical experiments for one and two-dimensional scalar and systems problems confirm the high order accuracy and good quality of our scheme.

Key Words: High order accuracy; Residual distribution; HWENO scheme; Conservation laws; Steady state.

¹School of Mathematical Sciences, Hangzhou, Zhejiang University, Zhejiang 310058, P.R. China. jianfang.lin@zju.edu.cn

²School of Mathematical Sciences, Xiamen University, Xiamen, Fujian 361005, P.R. China. ypren@stu.xmu.edu.cn

³Institute of Mathematics, University of Zurich, Zurich 8057, Switzerland. remi.abgrall@math.uzh.ch

⁴School of Mathematical Sciences and Fujian Provincial Key Laboratory of Mathematical Modeling and High-Performance Scientific Computing, Xiamen University, Xiamen, Fujian 361005, P.R. China. jxqiu@xmu.edu.cn

1 Introduction

In this paper, we propose a new type of the residual distribution (RD) conservative finite difference Hermite weighted essentially non-oscillatory (HWENO) method for solving the following steady state hyperbolic conservation laws

$$\nabla \cdot F(u) = 0, \quad (1.1)$$

where hyperbolicity means that $\frac{\partial F(u)}{\partial u} \cdot \xi$ is diagonal with real eigenvalues for any real vector ξ . The RD scheme has received considerable attention and been successfully used to solve steady state problems in [1, 4, 19].

The RD schemes are composed of two parts: residual (or fluctuation) evaluation and residual distribution. A brief framework of the RD scheme for a two-dimensional steady state problems (1.1) is introduced as follows: given a general triangular or quadrilateral mesh \mathcal{T}_h , nodes $\{M_i\}_{i=1, \dots, n_s}$ of \mathcal{T}_h , and T is a generic element. On each element T , we should define a total residual Φ^T and Φ_i^T , which is the amount of Φ^T associated with the vertex M_i , such that a conservation property is satisfied

$$\Phi^T = \int_T \nabla \cdot F^h(u_h) dx, \quad \sum_{i, M_i \in T} \Phi_i^T = \Phi^T, \quad (1.2)$$

where $|C_i|$ is the area of the dual element associated with the vertex M_i . The accuracy can be obtained at steady state when vanishing cell residuals. The class of RD schemes, or fluctuation splitting schemes were pioneered and developed by Roe, Sidikover, Deconinck, Struijs and their collaborators [31, 26, 14, 5, 4, 7, 8, 4, 6, 13]. In the past decades of the development, the RD scheme has demonstrated its robustness in many numerical experiments and does not have the restriction on the regularity of the mesh. The Lax-Wendroff theorem in [5] has proved that the numerical solution of the RD scheme is convergent to the weak solution, if the flux function satisfies the Lipschitz continuity. And the stability of the RD scheme can be obtained by the maxima principle, see [1, 7]. The accuracy of the scheme is reached at steady state when residues vanishing, if the residual property in [1] holds. Above the work of the RD scheme, it is at most second order accuracy. Later on, Abgrall and Roe [8] extend the RD scheme to a higher order in triangle meshes. Also, Abgrall and Meapeau consider the construct of the second order RD scheme in quadrilateral meshes. Besides for the steady state problems, the RD scheme is also applied for solving unsteady state problems, see [6, 13]. Abgrall and his collaborators in [3, 2] extend the RD scheme to the

multi-dimensional systems.

Due to the fact that the steady state problem (1.1) would exhibit hyperbolic behavior, for instance, shock and other discontinuities, it's necessary to develop a numerical scheme with capable of capturing these traits. Weighted essentially non-oscillatory (WENO) scheme [29, 30, 17] has been widely studied to solve hyperbolic conservation laws with good properties of high order accuracy in smooth regions and non-oscillatory near discontinuity. In particular, Chou and Shu in [11, 12] propose a new RD scheme combined with WENO scheme. Recently, high order Hermite WENO (HWENO) methods [22, 18] have gained many attention in solving hyperbolic conservation laws. Both the traditional WENO and HWENO methods can achieve the high order accuracy and preserve the essentially non-oscillatory property, but the HWENO scheme uses the Hermite interpolation in reconstructing polynomials, that involves both the unknown variable and its first order spatial derivative or first moment. Thus, the HWENO reconstruction stencil becomes more compact and their boundary treatment is much simpler, although more storage and some additional work are needed to evaluate the spatial derivatives. The HWENO scheme was first introduced in the construction of a limiter for the DG method [20, 21] due to its compact stencil. It was first used to solve the time-dependent Hamilton-Jacobi equation in [22], and the numerical results show that the HWENO scheme has smaller errors than the traditional WENO method on the same mesh and order. Since then, many HWENO schemes have been developed to solve hyperbolic conservation laws [18, 32, 33, 34, 36] on structured and triangular meshes. In addition, it is observed in [24] that the finite volume HWENO scheme enjoys the asymptotic preserving property, when applied to the steady-state discrete ordinates (S_N) transport equation.

In this paper, built upon the high order RD schemes and HWENO reconstructions, we design a sixth order RD conservative HWENO scheme for solving steady state hyperbolic conservation laws. It is worth mentioning that we are no longer using the traditional HWENO framework, namely, using one equation to update original variables u and several additional auxiliary equations to update its derivatives. Instead, we use the new approach presented in recent work [23], to use only one equation to update original variables. The derivatives of u will be obtained from applying the HWENO reconstruction on the updated values of u and the previous values of the derivatives. This approach saves the computational storage and CPU costs, which improves the computational efficiency of the traditional HWENO scheme.

The paper is organized as follows. In Section 2 and 3, we formulate the residual evaluation and the residual distribution procedures for one and two-dimensional problems, respectively. The performance of proposed method is shown in Section 4, through extensive numerical tests on several benchmark problems for steady state simulations. Finally, concluding remarks are given in Section 5.

2 High order RD conservative finite difference HWENO scheme in one dimension

In this section, we develop a high order RD finite difference HWENO scheme for steady state hyperbolic conservation laws in one dimension. In the first subsection, we define the total residual within each interval through the integral form, and then describe the distribution of total residual within each interval, complying with the principles of upwind scheme and the residual property. In the second subsection, we generalize the scheme to one-dimensional systems, based on a local characteristic field decomposition and using the same principles as in the scalar case to distribute the total residual within each interval in the characteristic fields.

2.1 One-dimensional scalar problem

We consider a one-dimensional scalar steady state problem

$$f(u)_x = s(u, x). \quad (2.1)$$

On the uniform grid $\{x_i\}_{i=1, \dots, N}$ with constant $\Delta x = x_{i+1} - x_i$, we define the grid function to be $\{u_i\}_{i=1, \dots, N}$, the interval $I_{i+\frac{1}{2}} = [x_i, x_{i+1}]$, the control volume $C_i = [x_{i-\frac{1}{2}}, x_{i+\frac{1}{2}}]$ and $x_{i+\frac{1}{2}} = \frac{x_i + x_{i+1}}{2}$, and the length of C_i is denoted by $|C_i|$, which is equal to Δx .

The total residual in the interval $I_{i+\frac{1}{2}}$ is defined by

$$\Phi_{i+\frac{1}{2}} = \int_{x_i}^{x_{i+1}} (f(u)_x - s(u, x)) dx = f(u_{i+1}) - f(u_i) - \int_{x_i}^{x_{i+1}} s(u, x) dx. \quad (2.2)$$

If we can reach the zero residual limit, i.e. $\Phi_{i+\frac{1}{2}} = 0$ for all i , then the accuracy of the scheme is determined by the accuracy of the approximation to $\int_{x_i}^{x_{i+1}} s(u, x) dx$. In our scheme, we develop a sixth order HWENO integration to approximate the integral $\int_{x_i}^{x_{i+1}} s(u, x) dx$. Note that the HWENO integration also uses the spatial derivative of the point value u and here we denote its spatial derivative u_x as v . Later on, we will use the current u and the old v to update v , instead

of introducing additional equations for v , which is commonly applied in the traditional HWENO methods. We now explain the procedure of the sixth order HWENO integration.

Step 1. Choose a big stencil $S_0 = \{x_{i-1}, x_i, x_{i+1}, x_{i+2}\}$, and construct a fifth degree polynomial $p_0(x)$ on it, satisfying

$$\begin{cases} p_0(x_{i+l}) = s_{i+l}, & l = -1, 0, 1, 2, \\ p_0'(x_{i+l}) = s'_{i+l}, & l = 0, 1. \end{cases} \quad (2.3)$$

And also choose three small stencils $S_1 = \{x_{i-1}, x_i, x_{i+1}\}$, $S_2 = \{x_i, x_{i+1}, x_{i+2}\}$ and $S_3 = \{x_{i-1}, x_i, x_{i+1}, x_{i+2}\}$, and construct cubic polynomials p_1 , p_2 and p_3 on these stencils respectively, which satisfy

$$\begin{cases} p_1(x_{i+l}) = s_{i+l}, & l = -1, 0, 1, \\ p_1'(x_i) = s'_i, \end{cases} \quad (2.4)$$

$$\begin{cases} p_2(x_{i+l}) = s_{i+l}, & l = 0, 1, 2, \\ p_2'(x_{i+1}) = s'_{i+1}, \end{cases} \quad (2.5)$$

and

$$p_3(x_{i+l}) = s_{i+l}, \quad l = -1, 0, 1, 2. \quad (2.6)$$

where

$$\begin{cases} s_{i+l} = s(u_{i+l}, x_{i+l}), & l = -1, 0, 1, 2, \\ s'_{i+l} = s'(u_{i+l}, x_{i+l}) = \left(\frac{\partial s}{\partial u} v + \frac{\partial s}{\partial x} \right) \Big|_{x=x_{i+l}}, & l = 0, 1. \end{cases}$$

And then integrate the above polynomials $p_0(x)$, $p_1(x)$, p_2 , $p_3(x)$ over the interval $I_{i+\frac{1}{2}}$, and are denoted by q_0 , q_1 , q_2 , q_3 , respectively. In particular, we have

$$\begin{aligned} q_0 &= \frac{\Delta x}{240}(s_{i-1} + 119s_i + 119s_{i+1} + s_{i+2} + 22\Delta x s'_i - 22\Delta x s'_{i+1}), \\ q_1 &= \frac{\Delta x}{24}(s_{i-1} + 16s_i + 7s_{i+1} + 6\Delta x s'_i), \\ q_2 &= -\frac{\Delta x}{24}(-7s_i - 16s_{i+1} - s_{i+2} + 6\Delta x s'_{i+1}), \\ q_3 &= \frac{\Delta x}{24}(-s_{i-1} + 13s_i + 13s_{i+1} - s_{i+2}), \end{aligned}$$

Step 2. Compute the combination coefficients of $q_l, l = 1, 2, 3$, such that

$$q_0 = \sum_{l=1}^3 \gamma_l q_l, \quad (2.7)$$

which are called linear weights. Therefore, we obtain

$$\gamma_1 = \frac{11}{30}, \quad \gamma_2 = \frac{11}{30}, \quad \gamma_3 = \frac{4}{15}. \quad (2.8)$$

Step 3. Compute the smoothness indicators $\beta_l, l = 1, 2, 3$, which measure how smooth the functions $p_l, l = 1, 2, 3$ are in the target interval $I_{i+\frac{1}{2}}$. The smaller these smoothness indicators, the smoother the functions are in the interval $I_{i+\frac{1}{2}}$. We use the same recipe for the smoothness indicators as in [9, 17, 28].

$$\beta_l = \sum_{m=1}^{r_0} \int_{I_{i+\frac{1}{2}}} \Delta x^{2m-1} \left(\frac{d^m p_l}{dx^m} \right)^2 dx, \quad l = 1, 2, 3, \quad (2.9)$$

where $r_0 = 3$ is the corresponding degree of the polynomial. In particular, we have

$$\begin{aligned} \beta_1 &= \frac{301}{30} (s_{i-1} + \frac{65}{602} s_i - \frac{667}{602} s_{i+1} + \frac{1269}{602} \Delta x s'_i)^2 \\ &\quad + \frac{12561}{2408} (s_i - s_{i+1} + \frac{10153}{12561} \Delta x s'_i)^2 + \frac{10153}{12561} (\Delta x s'_i)^2, \\ \beta_2 &= \frac{301}{30} (-\frac{667}{602} s_i + \frac{65}{602} s_{i+1} + s_{i+2} - \frac{1269}{602} \Delta x s'_{i+1})^2 \\ &\quad + \frac{12561}{2408} (-s_i + s_{i+1} - \frac{10153}{12561} \Delta x s'_{i+1})^2 + \frac{10153}{12561} (\Delta x s'_{i+1})^2, \\ \beta_3 &= \frac{61}{45} (s_{i-1} - \frac{1269}{488} s_i + \frac{537}{244} s_{i+1} - \frac{293}{488} s_{i+2})^2 \\ &\quad + \frac{21865}{11712} (s_i - \frac{32018}{21865} s_{i+1} + \frac{10153}{21865} s_{i+2})^2 + \frac{10153}{21865} (s_{i+1} - s_{i+2})^2. \end{aligned}$$

Step 4. Calculate the non-linear weights based on the linear weights and the smoothness indicators. They are defined as follows:

$$\omega_l = \frac{\bar{\omega}_l}{\sum_{m=1}^3 \bar{\omega}_m}, \quad \bar{\omega}_k = \frac{\gamma_l}{(\varepsilon + \beta_l)^2}, \quad l = 1, 2, 3. \quad (2.10)$$

And it is easy to verify that $\omega_l = \gamma_l + \mathcal{O}(\Delta x^3)$ when the solution is smoothness. In our numerical experiments, we take $\varepsilon = 10^{-10}$.

Step 5. The sixth order reconstruction of the integral $\int_{x_i}^{x_{i+1}} s(u, x) dx$ is obtained by

$$\int_{x_i}^{x_{i+1}} s(u, x) dx = \sum_{m=1}^3 \omega_m q_m + \mathcal{O}(\Delta x^7), \quad (2.11)$$

when the solution is smoothness.

Remark 2.1. The sixth order HWENO integration leads to the seventh order HWENO approximation to the integral $\int_{x_i}^{x_{i+1}} s(u, x) dx$ within each interval and hence the sixth order approximation to the integral over the whole computational domain.

Next we start to distribute the total residuals. In the interval $[x_i, x_{i+1}]$, the total residual is $\Phi_{i+\frac{1}{2}}$, and it is distributed to the nodes x_i and x_{i+1} as $\Phi_{i+\frac{1}{2}}^1$ and $\Phi_{i+\frac{1}{2}}^2$. For simplicity and with no ambiguity, we drop off the subscript $i + \frac{1}{2}$ for the total residual $\Phi_{i+\frac{1}{2}}$. We require that $\Phi = \Phi^1 + \Phi^2$ for the conservation and $|\Phi^k|/|\Phi|, k = 1, 2$ be uniformly bounded by the residual property [1]. One way to distribute the total residual Φ with upwinding property is given by

$$\Phi^1 = (1 - \alpha)\Phi, \quad \Phi^2 = \alpha\Phi, \quad \alpha \in [0, 1], \quad (2.12)$$

with α defined by

$$\alpha = \begin{cases} 1 & \text{if } \bar{\lambda} \geq \delta, \\ 0 & \text{if } \bar{\lambda} \leq -\delta, \\ r(\bar{\lambda}, \delta) & \text{otherwise,} \end{cases}$$

where $\bar{\lambda} = f'(\bar{u})$, and \bar{u} are an average state in the interval taken to be $\frac{1}{2}(u_i + u_{i+1})$. The function $r(\cdot, \cdot)$ is a continuous differentiable entropy function for the Roe scheme [16], which is given by

$$r(\lambda, \delta) = \frac{1}{4\delta^3}(\lambda + \delta)^2(2\delta - \lambda), \quad (2.13)$$

where the coefficient δ is chosen accordingly in the problem.

And the point value u_i^{new} is updated through sending the distributed residuals to the point x_i , as in a pseudo time-marching scheme, which can be written as a semi-discrete system

$$\frac{du_i^{\text{new}}}{dt} + \frac{1}{|C_i|} \left(\Phi_{i-\frac{1}{2}}^2 + \Phi_{i+\frac{1}{2}}^1 \right) = 0. \quad (2.14)$$

In our numerical experiments, we use a forward Euler scheme for the pseudo time discretization.

For the spatial derivative of the point value v_i^{new} , we use the current point value u and the old spatial derivative v^{old} to update it. We adopt a fourth order HWENO reconstruction proposed in [35]. We now roughly review the procedure of the reconstruction. For simplification, we denote v^{old} by v .

step 1. Choose three stencils $S_1 = \{x_{i-1}, x_i\}$, $S_2 = \{x_i, x_{i+1}\}$, $S_3 = \{x_{i-1}, x_i, x_{i+1}\}$, and a big stencil $S_0 = \{x_{i-1}, x_i, x_{i+1}\} = S_3$. Then construct three quadratic polynomials $P_1(x)$, $P_2(x)$ and $P_3(x)$ on S_1 , S_2 and S_3 by Hermite interpolation, respectively, under the following conditions

$$P_1(x_{i+l}) = u_{i+l}, \quad l = -1, 0, \quad P_1'(x_{i-1}) = v_{i-1},$$

$$P_2(x_{i+l}) = u_{i+l}, \quad l = 0, 1, \quad P_2'(x_{i+1}) = v_{i+1},$$

$$P_3(x_{i+l}) = u_{i+l}, \quad l = -1, 0, 1.$$

Similarly, a quartic polynomial P_0 is also obtained by Hermite interpolation, satisfying

$$P_0(x_{i+l}) = u_{i+l}, \quad l = -1, 0, 1, \quad P_0'(x_{i+l}) = v_{i+l}, \quad l = -1, 1.$$

Therefore, we get their derivative values at the point x_i as follows:

$$\begin{aligned} P_1'(x_i) &= -v_{i-1} + \frac{2(u_i - u_{i-1})}{\Delta x}, \\ P_2'(x_i) &= -v_{i+1} + \frac{2(u_{i+1} - u_i)}{\Delta x}, \\ P_3'(x_i) &= \frac{u_{i+1} - u_{i-1}}{\Delta x}, \\ P_0'(x_i) &= -\frac{v_{i-1} + v_{i+1}}{4} + \frac{3(u_{i+1} - u_{i-1})}{4\Delta x}. \end{aligned}$$

Step 2. Compute the linear weights $\gamma_l, l = 1, 2, 3$ by requiring that

$$P_0'(x_i) = \sum_{l=1}^3 \gamma_l P_l'(x_i),$$

then we have

$$\gamma_1 = \frac{1}{4}, \quad \gamma_2 = \frac{1}{4}, \quad \gamma_3 = \frac{1}{2}.$$

Step 3. Compute the smoothness indicators $\beta_l, l = 1, 2, 3$ to measure how smooth the functions $P_l(x), l = 1, 2, 3$ are in the target cell C_i , defined in the following

$$\beta_l = \sum_{m=1}^{r_0} \int_{C_i} \Delta x^{2m-1} \left(\frac{d^m P_l}{dx^m} \right)^2 dx \quad (2.15)$$

Where $r_0 = 2$ is the degree of the polynomials $P_l, l = 1, 2, 3$. In particular, we have

$$\begin{aligned} \beta_1 &= (2u_i - 2u_{i-1} - v_{i-1}\Delta x)^2 + \frac{13}{3}(u_i - u_{i-1} - v_{i-1}\Delta x)^2, \\ \beta_2 &= (2u_{i+1} - 2u_i - v_{i+1}\Delta x)^2 + \frac{13}{3}(u_{i+1} - u_i - v_{i+1}\Delta x)^2, \\ \beta_3 &= \frac{1}{4}(u_{i+1} - u_{i-1})^2 + \frac{13}{12}(u_{i-1} - 2u_i + u_{i+1})^2. \end{aligned}$$

Step 4. The nonlinear weights are obtained as

$$\omega_l = \frac{\bar{\omega}_l}{\sum_{m=1}^3 \bar{\omega}_m}, \quad \bar{\omega}_l = \frac{\gamma_l}{(\beta_l + \varepsilon)^2}, \quad l = 1, 2, 3, \quad (2.16)$$

where ε is taken to be 10^{-10} to avoid denominator being zero. Therefore, the derivative value v_i^{new} is obtained by

$$v_i^{\text{new}} = \sum_{l=1}^3 \omega_l P_l'(x_i). \quad (2.17)$$

2.2 One-dimensional systems

Consider a one-dimensional steady state system (2.1), where \mathbf{u} , $\mathbf{f}(\mathbf{u})$ and $\mathbf{s}(\mathbf{u}, x)$ are vector-valued functions in \mathbb{R}^m . For hyperbolic systems, we assume that the Jacobian matrix $\mathbf{f}'(\mathbf{u})$ can be written as $R\Lambda L$, where Λ is a diagonal matrix with real eigenvalues on the diagonal, and L and R are matrices of left and right eigenvectors of $\mathbf{f}'(\mathbf{u})$, respectively.

The grid, grid function, the interval, and control volume are denoted as in Subsection 2.1. The total residual $\Phi_{i+\frac{1}{2}}$ in the interval $[x_i, x_{i+1}]$ is again defined by (2.2). As before, the accuracy of the scheme is determined by the accuracy of the approximation to $\int_{x_i}^{x_{i+1}} \mathbf{s}(\mathbf{u}, x) dx$, which is again approximated by the sixth order HWENO integration.

In order to distribute the total residual $\Phi_{i+\frac{1}{2}}$, we need to use a local characteristic decomposition in the interval $[x_i, x_{i+1}]$. First, we compute an average state $\bar{\mathbf{u}}$ between \mathbf{u}_i and \mathbf{u}_{i+1} , using either the simple arithmetic mean or Roe's average [25] and \bar{L} and \bar{R} are the corresponding left and right eigenvectors L and R evaluated at the average state $\bar{\mathbf{u}}$, and $\bar{\lambda}_k$ is the corresponding k -th eigenvalue. In the following, for simplicity and with no ambiguity, we drop off the subscript $i + \frac{1}{2}$ for the total residual $\Phi_{i+\frac{1}{2}}$. To keep the conservation, we require that $\Phi = \Phi^1 + \Phi^2$ and $|\Phi^k|/|\Phi|, k = 1, 2$, which is in a component by component sense and similar to the one-dimensional scalar cases, be uniformly bounded to guarantee the residual property [1]. Now we project total residual Φ at the interval to the characteristic field, namely, $\Psi = \bar{L}\Phi$, then distribute the residual Ψ to the nodes x_i and x_{i+1} in the upwinding way, denoted by Ψ^1 and Ψ^2 , and we obtain that $\Psi = \Psi^1 + \Psi^2$. According to one-dimensional scalar problem, the upwind scheme can be defined naturally in the following:

$$\Psi^1 = (\mathbf{I} - \Sigma)\Psi, \quad \Psi^2 = \Sigma\Psi, \quad (2.18)$$

where \mathbf{I} is an identity matrix, Σ is a diagonal matrix, and the k -th diagonal component of Σ is given by

$$\Sigma_{kk} = \begin{cases} 1 & \text{if } \bar{\lambda}_k \geq \delta, \\ 0 & \text{if } \bar{\lambda}_k \leq -\delta, \\ r(\bar{\lambda}_k, \delta) & \text{otherwise.} \end{cases}$$

The function $r(\cdot, \cdot)$ is defined as (2.13), and δ is also chosen accordingly in the problem.

And we need to project the residuals Ψ^1 and Ψ^2 back to the physical space and then obtain the residuals distributed to the nodes x_i and x_{i+1} as follows:

$$\Phi^1 = \bar{R}\Psi^1, \quad \Phi^2 = \bar{R}\Psi^2. \quad (2.19)$$

Thus, we get the way to distribute the total residual within each interval. As in the scalar case, the point value $\mathbf{u}_i^{\text{new}}$ can be updated in the pseudo time-marching semi-discrete scheme (2.14), which is again discretized by a forward Euler scheme in our numerical experiments until the steady state is reached. And for $\mathbf{v}_i^{\text{new}}$, it is again constructed by the fourth order HWENO reconstruction as explained in the Subsection 2.1 component by component.

3 High order RD conservative finite difference HWENO scheme in two dimensions

In this section, we develop a high order RD finite difference HWENO scheme for two-dimensional steady state problems. More precisely, we focus on our scheme on uniform meshes. In Subsection 3.1, we define the total residual within each cell through the integral form, as defined in (2.2), and then introduce the residual distribution mechanism. In Subsection 3.2, we extend the scheme to two-dimensional systems, which is based on a local characteristic field decomposition, and distribution the total residuals in characteristic fields dimension by dimension.

3.1 Two-dimensional scalar problems

We consider a two-dimensional scalar steady state problem

$$f(u)_x + g(u)_y = s(u, x, y). \quad (3.1)$$

On the uniform grid to be $\{(x_i, y_j)\}_{\substack{i=1, \dots, N \\ j=1, \dots, M}}$ with constant $\Delta x = x_{i+1} - x_i$ and $\Delta y = y_{j+1} - y_j$, we define the grid function to be u_{ij} , the cell $I_{i+\frac{1}{2}, j+\frac{1}{2}} = [x_i, x_{i+1}] \times [y_j, y_{j+1}]$, the control volume $C_{ij} = [x_{i-\frac{1}{2}}, x_{i+\frac{1}{2}}] \times [y_{j-\frac{1}{2}}, y_{j+\frac{1}{2}}]$, and $x_{i+\frac{1}{2}} = \frac{x_i + x_{i+1}}{2}$ and $y_{j+\frac{1}{2}} = \frac{y_j + y_{j+1}}{2}$, and the area of C_{ij} is denoted by $|C_{ij}|$, which is equal to $\Delta x \cdot \Delta y$.

The total residual in the cell $I_{i+\frac{1}{2}, j+\frac{1}{2}}$ is defined by

$$\begin{aligned} \Phi_{i+\frac{1}{2}, j+\frac{1}{2}} &= \int_{y_j}^{y_{j+1}} \int_{x_i}^{x_{i+1}} (f(u)_x + g(u)_y - s(u, x, y)) \, dx \, dy \\ &= \int_{y_j}^{y_{j+1}} (f(u(x_{i+1}, y)) - f(u(x_i, y))) \, dy \\ &\quad + \int_{x_i}^{x_{i+1}} (g(u(x, y_{j+1})) - g(u(x, y_j))) \, dx \\ &\quad - \int_{y_j}^{y_{j+1}} \int_{x_i}^{x_{i+1}} s(u(x, y), x, y) \, dx \, dy. \end{aligned} \quad (3.2)$$

If we can reach the zero residual limit, i.e., $\Phi_{i+\frac{1}{2},j+\frac{1}{2}} = 0$ for all i and j , the accuracy of the scheme is determined by the accuracy of the approximations to the integrations of the fluxes and the source term.

To approximate the integrations of the fluxes, which are one-dimensional integrals, we use the sixth order HWENO integration as described in Subsection 2.1. As for the source term $\int_{y_j}^{y_{j+1}} \int_{x_i}^{x_{i+1}} s(u, x, y) dx dy$, we approximate it in a dimension by dimension fashion, which is explained as follows.

First, we define

$$S_{i+\frac{1}{2}}(y) = \int_{x_i}^{x_{i+1}} s(u(x, y), x, y) dx,$$

$$(S_{i+\frac{1}{2}}(y))_y = \int_{x_i}^{x_{i+1}} s(u(x, y), x, y)_y dx,$$

and then the integral of the source term in the cell $I_{i+\frac{1}{2},j+\frac{1}{2}}$ can be rewritten as

$$\int_{y_j}^{y_{j+1}} \int_{x_i}^{x_{i+1}} s(u(x, y), x, y) dx dy = \int_{y_j}^{y_{j+1}} S_{i+\frac{1}{2}}(y) dy.$$

The integral $\int_{y_j}^{y_{j+1}} S_{i+\frac{1}{2}}(y) dy$ can be approximated by the sixth order HWENO integration in the y -direction, using $\{S_{i+\frac{1}{2}}(y_{j+k})\}_{k=-1, \dots, 2}$ and $\{(S_{i+\frac{1}{2}}(y_{j+k}))_y\}_{k=0,1}$. By the definition of $S_{i+\frac{1}{2}}(y)$ and $(S_{i+\frac{1}{2}}(y))_y$, $S_{i+\frac{1}{2}}(y_{j+k})$ can again be approximated by the sixth order HWENO integration in the x -direction, using $\{s(u_{i+l,j+k}, x_{i+l}, y_{j+k})\}_{l=-1, \dots, 2}$ and $\{s(u_{i+l,j+k}, x_{i+l}, y_{j+k})_x\}_{l=0,1}$. Similarly, $(S_{i+\frac{1}{2}}(y))_y$ can be approximated by the sixth order HWENO integration in the x -direction, using $\{s(u_{i+l,j+k}, x_{i+l}, y_{j+k})_y\}_{l=-1, \dots, 2}$ and $\{s(u_{i+l,j+k}, x_{i+l}, y_{j+k})_xy\}_{l=0,1}$. Thus, the integration of the source term can be approximated dimension by dimension, and the sixth order accuracy is obtained at the zero residual limit.

Remark 3.1. According to the above, we still need the information of the spatial derivatives u_x and u_y and the second cross derivative u_{xy} , and denoted by v , w and z , respectively.

Next, we start to distribute the total residuals. In the cell $I_{i+\frac{1}{2},j+\frac{1}{2}} = [x_i, x_{i+1}] \times [y_j, y_{j+1}]$, the total residual is $\Phi_{i+\frac{1}{2},j+\frac{1}{2}}$, and it is to be distributed to the vertices of the cell, which are denoted to be $M_1 = (x_i, y_j)$, $M_2 = (x_{i+1}, y_j)$, $M_3 = (x_i, y_{j+1})$ and $M_4 = (x_{i+1}, y_{j+1})$. Here we denote the residuals distributed to the vertices M_k as $\Phi_{i+\frac{1}{2},j+\frac{1}{2}}^k$, $k = 1, 2, 3, 4$. For simplicity and without ambiguity, we drop off the subscript $(i + \frac{1}{2}, j + \frac{1}{2})$ in the notations. For the conservation and the

residual property in [1], we require that $\Phi = \sum_{k=1}^4 \Phi^k$ and $|\Phi^k|/|\Phi|, k = 1, \dots, 4$ be uniformly bounded.

In order to have an upwinding property, we have the upwind scheme in the following

$$\tilde{\Phi}^1 = (1 - \alpha)((1 - \beta))\Phi, \quad \tilde{\Phi}^2 = \alpha(1 - \beta)\Phi, \quad \tilde{\Phi}^3 = (1 - \alpha)\beta\Phi, \quad \tilde{\Phi}^4 = \alpha\beta\Phi, \quad (3.3)$$

with $\alpha, \beta \in [0, 1]$. α is the coefficient for upwinding in the x -direction, which is given by

$$\alpha = \begin{cases} 1 & \text{if } \bar{\lambda}_x \geq \delta, \\ 0 & \text{if } \bar{\lambda}_x \leq -\delta, \\ r(\bar{\lambda}_x, \delta) & \text{otherwise,} \end{cases}$$

where $\bar{\lambda}_x = f'(\bar{u})$, and \bar{u} is an average state in the cell $I_{i+\frac{1}{2}, j+\frac{1}{2}}$ to taken by

$$\bar{u} = \frac{1}{4}(u_{i,j} + u_{i+1,j} + u_{i,j+1} + u_{i+1,j+1}).$$

Similarly, β is the coefficient for upwinding in the y -direction, which is given by

$$\beta = \begin{cases} 1 & \text{if } \bar{\lambda}_y \geq \delta, \\ 0 & \text{if } \bar{\lambda}_y \leq -\delta, \\ r(\bar{\lambda}_y, \delta) & \text{otherwise,} \end{cases}$$

where $\bar{\lambda}_y = g'(\bar{u})$. And the function $r(\cdot, \cdot)$ is given as in (2.13), δ is chosen accordingly in the problem.

Our numerical experiments show that for shock problems, it is necessary to add dissipation term for the stability of the scheme proposed. Thus, we introduce an additional dissipation residual Φ_{diss}^k to the residual $\tilde{\Phi}^k$ for each vertex. Here is the definition of dissipation residual in the following:

$$\begin{aligned} \Phi_{\text{diss}}^1 &= \frac{\sigma}{2}\Delta^3 \left(\frac{u_{i,j} - u_{i+1,j}}{\Delta x} + \frac{u_{i,j} - u_{i,j+1}}{\Delta y} \right), \\ \Phi_{\text{diss}}^2 &= \frac{\sigma}{2}\Delta^3 \left(\frac{u_{i+1,j} - u_{i,j}}{\Delta x} + \frac{u_{i+1,j} - u_{i+1,j+1}}{\Delta y} \right), \\ \Phi_{\text{diss}}^3 &= \frac{\sigma}{2}\Delta^3 \left(\frac{u_{i,j+1} - u_{i+1,j+1}}{\Delta x} + \frac{u_{i,j+1} - u_{i,j}}{\Delta y} \right), \\ \Phi_{\text{diss}}^4 &= \frac{\sigma}{2}\Delta^3 \left(\frac{u_{i+1,j+1} - u_{i,j+1}}{\Delta x} + \frac{u_{i+1,j+1} - u_{i+1,j}}{\Delta y} \right), \end{aligned} \quad (3.4)$$

where $\Delta = \max(\Delta x, \Delta y)$, and σ is chosen accordingly in the problem. This dissipation mechanism works well for our numerical experiments, but it may not be the optimal approach, since it has a adjustable coefficient σ , whose choice for optimal performance seems to be problem dependent.

Thus, we get the way to distribute the total residual within each cell and obtained by

$$\Phi^k = \tilde{\Phi}^k + \Phi_{\text{diss}}^k, \quad k = 1, \dots, 4. \quad (3.5)$$

The point value u_{ij}^{new} is then updated through sending the distributed residuals to the point (x_i, y_j) , as in a pseudo time-marching scheme, which can be written as a semi-discrete system

$$\frac{du_{ij}^{\text{new}}}{dt} + \frac{1}{|C_{ij}|} \left(\Phi_{i+\frac{1}{2}, j+\frac{1}{2}}^1 + \Phi_{i-\frac{1}{2}, j+\frac{1}{2}}^2 + \Phi_{i+\frac{1}{2}, j-\frac{1}{2}}^3 + \Phi_{i-\frac{1}{2}, j-\frac{1}{2}}^4 \right) = 0. \quad (3.6)$$

We again use a forward Euler scheme for the pseudo time discretization. And we may lose the strict residual property after adding dissipation residuals, but note that conservation is still preserved after adding the dissipation since $\sum_{k=1}^4 \Phi_{\text{diss}}^k = 0$.

For the spatial derivatives v^{new} and w^{new} , they can be approximated by the fourth order HWENO reconstruction in the x -direction and the y -direction, respectively, as introduced in the Subsection 2.1. For the second cross derivative z^{new} , it is updated by dimension-by-dimension, we first consider u_x approximated by the fourth order HWENO reconstruction in the x -direction and then $(u_x)_y$ again by the fourth order HWENO reconstruction in the y -direction, and thus we can update z^{new} .

3.2 Two-dimensional systems

Consider a two-dimensional steady state system (3.1), where \mathbf{u} , $\mathbf{f}(\mathbf{u})$, $\mathbf{g}(\mathbf{u})$ and $\mathbf{s}(\mathbf{u}, x, y)$ are vector-valued functions in \mathbb{R}^m . For hyperbolic systems, we assume that any real linear combination of the Jacobians $n_x \mathbf{f}'(\mathbf{u}) + n_y \mathbf{g}'(\mathbf{u})$ is diagonalizable with real eigenvalues. In particular, we assume $\mathbf{f}'(\mathbf{u})$ and $\mathbf{g}'(\mathbf{u})$ can be written as $R_x \Lambda_x L_x$ and $R_y \Lambda_y L_y$, respectively, where Λ_x and Λ_y are diagonal matrices with real eigenvalues on the diagonal, and L_x, R_x and L_y, R_y are matrices of left and right eigenvectors for the corresponding Jacobians.

The grid, grid function, cell and control volume are denoted as in Subsection 3.1. The total residual in the cell $I_{i+\frac{1}{2}, j+\frac{1}{2}} = [x_i, x_{i+1}] \times [y_j, y_{j+1}]$ is still defined by (3.2). As before, if we can reach the zero residual limit of the scheme, the accuracy of the scheme is determined by the accuracy of the approximations to the integrals of the fluxes and the source term. We again use the sixth order HWENO integration as described in Subsection 2.1. For simplicity and without ambiguity, we drop off the subscript $(i + \frac{1}{2}, j + \frac{1}{2})$ in the notations in the following.

We need to distribute the total residual Φ to the four vertices $\{M_k\}_{k=1, \dots, 4}$, which is defined in Subsection 3.1 and the corresponding residuals are still denoted by $\{\Phi^k\}_{k=1, \dots, 4}$, where $\Phi^k \in \mathbb{R}^m$. We require that $\Phi = \sum_{k=1}^4 \Phi^k$ and $|\Phi^k|/|\Phi|, k = 1, \dots, 4$, which is in a component by component sense and similar to the two-dimensional scalar cases, should be uniformly bounded

for the conservation and residual property in [1]. Here we consider a dimension by dimension procedure, coupled with a local characteristic field decomposition. First, we compute an average state $\bar{\mathbf{u}}$ in $I_{i+\frac{1}{2},j+\frac{1}{2}}$, using either arithmetic mean or Roe's average [25], and denote \bar{L}_x and \bar{R}_x as the matrices with left and right eigenvectors L_x and R_x of $\mathbf{f}'(\mathbf{u})$ evaluated at the average state $\bar{\mathbf{u}}$, and $\bar{\lambda}_x^k$ are the corresponding eigenvalues; \bar{L}_y , \bar{R}_y and $\bar{\lambda}_y^k$ are defined similarly but associated with L_y , R_y and Λ_y of $\mathbf{g}'(\mathbf{u})$.

We now explain how to distribute the total residual within each cell dimension by dimension in the upwinding way.

Step 1. Consider the y -direction, and project the residual Φ to the local characteristic field in the y -direction, we have $\Psi = \bar{L}_y \Phi$. Then the residual Ψ is distributed to the nodes y_j and y_{j+1} in the y -direction, denoted by Ψ^1 and Ψ^2 , respectively, and $\Psi = \Psi^1 + \Psi^2$. Residuals $\Psi^{1,2}$ are defined by

$$\Psi^1 = (\mathbf{I} - \Sigma)\Psi, \quad \Psi^2 = \Sigma\Psi, \quad (3.7)$$

where \mathbf{I} is the identity matrix, Σ is a diagonal matrix with the k -th diagonal component given by

$$\Sigma_{kk} = \begin{cases} 1 & \text{if } \bar{\lambda}_y^k \geq \delta, \\ 0 & \text{if } \bar{\lambda}_y^k \leq -\delta, \\ r(\bar{\lambda}_y^k, \delta) & \text{otherwise.} \end{cases}$$

The function $r(\cdot, \cdot)$ is given in (2.13), and δ is also chosen accordingly in the problem.

And then project residuals $\Psi^{1,2}$ back to the physical space, we obtain residuals $\hat{\Phi}^{1,2}$, namely

$$\hat{\Phi}^1 = \bar{R}_y \Psi^1, \quad \hat{\Phi}^2 = \bar{R}_y \Psi^2. \quad (3.8)$$

Step 2. Consider the x -direction, and we would distribute the two parts $\hat{\Phi}^{1,2}$ in the x -direction. First we need to project residuals $\hat{\Phi}^{1,2}$ to the characteristic fields in the x -direction, namely

$$\Pi^1 = \bar{L}_x \hat{\Phi}^1, \quad \Pi^2 = \bar{L}_x \hat{\Phi}^2.$$

Then distribute residuals $\Pi^{1,2}$ in the x -characteristic fields. According to upwinding principle and residual property, we have

$$\bar{\Psi}^1 = (\mathbf{I} - \Gamma)\Pi^1, \quad \bar{\Psi}^2 = \Gamma\Pi^1, \quad \bar{\Psi}^3 = (\mathbf{I} - \Gamma)\Pi^2, \quad \bar{\Psi}^4 = \Gamma\Pi^2, \quad (3.9)$$

where \mathbf{I} is the identity matrix, and Γ is a diagonal matrix with the k -th diagonal component given by

$$\Gamma_{kk} = \begin{cases} 1 & \text{if } \bar{\lambda}_x^k \geq \delta, \\ 0 & \text{if } \bar{\lambda}_x^k \leq -\delta, \\ r(\bar{\lambda}_x^k, \delta) & \text{otherwise.} \end{cases}$$

The function $r(\cdot, \cdot)$ is given as in (2.13), and δ is chosen accordingly in the problem.

Step 3. Project distributed residuals $\{\bar{\Psi}^k\}_{k=1, \dots, 4}$ back to physical space, namely

$$\tilde{\Phi}^k = \bar{R}_x \bar{\Psi}^k, \quad k = 1, \dots, 4. \quad (3.10)$$

As in two dimensional scalar case, we need to add an additional dissipation residual $\Phi_{\text{diss}}^k, k = 1, \dots, 4$ to each of $\Phi^k, k = 1, \dots, 4$, and its definition is defined as in (3.4). Thus, we get the way to distribute the total residuals

$$\Phi^k = \tilde{\Phi}^k + \Phi_{\text{diss}}^k, \quad k = 1, \dots, 4. \quad (3.11)$$

The point value $\mathbf{u}_{ij}^{\text{new}}$ is updated through sending the distributed residuals to the point (x_i, y_j) , as in the pseudo time-marching scheme, which can be written as the semi-discrete systems (3.6). And we again use a forward Euler scheme for the pseudo time discretization in our numerical experiments until the steady state is reached. And for $\mathbf{v}_{ij}^{\text{new}}, \mathbf{w}_{ij}^{\text{new}}$ and $\mathbf{z}_{ij}^{\text{new}}$, they are again updated by the fourth order HWENO reconstruction component by component.

4 Numerical results

In this section, we present the numerical results of the proposed residual distribution conservative finite difference HWENO method for steady state conservation laws with source terms in scalar and system test problems in one and two dimensions. Pseudo time discretization towards steady state is by the Euler forward method in all numerical simulations. CFL number is taken to be 0.6 in one-dimensional cases and 0.2 in two-dimensional cases. In Subsection 4.1, for one-dimensional problems, the parameter δ in (2.13) for the Roe's entropy correction is taken as 0. In Subsection 4.2, for two-dimensional problems, δ is taken as 0 for scalar cases and 0.1 for system cases.

All the spatial discretizations in our numerical results are uniform and all numerical steady state is obtained with L^1 residue reduced to the round-off level.

4.1 The one-dimensional problems

Example 4.1. We solve the steady state solution of the one-dimensional Burgers equation with a source term:

$$\left(\frac{u^2}{2}\right)_x = \sin x \cos x \quad (4.1)$$

with the initial condition

$$u_0(x) = \beta \sin x, \quad (4.2)$$

and the boundary condition $u(0) = u(\pi) = 0$. This problem was studied in [27] as an example of multiple steady state solutions for characteristic initial value problems. The steady state solution to this problem depends on the value of β : if $-1 < \beta < 1$, a shock will form within the domain $[0, \pi]$; otherwise, the solution will be smooth at first, followed by a shock forming at the boundary $x = \pi$ ($\beta \geq 1$) or $x = 0$ ($\beta \leq -1$), and later converge to a smooth steady state $u(x, \infty) = \sin x$ ($\beta \geq 1$) or $u(x, \infty) = -\sin x$ ($\beta \leq -1$), respectively. In order to test the order of accuracy, we take $\beta = 2$ to have a smooth stationary solution. From the Table 4.1, we can clearly see that the sixth order accuracy is reached. In the Figure 4.1, we can observe that the L^1 error of the six order scheme using the HWENO integration is smaller than that of the sixth scheme using the WENO integration at the same grid.

Table 4.1: Errors and numerical orders of accuracy for the sixth order RD finite difference HWENO scheme for the Example 4.1.

N	L^1 error	Order	L^∞ error	Order
20	3.29E-08		4.92E-08	
40	5.02E-10	6.03	7.70E-10	6.00
80	7.75E-12	6.02	1.20E-11	6.00
160	1.20E-13	6.01	1.88E-13	6.00
320	1.88E-15	6.00	2.94E-15	6.00
640	2.93E-17	6.00	4.59E-17	6.00

Example 4.2. We consider the same problem as the Example 4.1, but here take $\beta = 0.5$ in the initial condition (4.2). As mentioned in the previous example, when $-1 < \beta < 1$, a shock will form within the domain, which separates two branches ($\sin x$ and $-\sin x$) of the steady state. The location of the shock is determined by the parameter β through conservation of mass ($\int_0^\pi u \, dx = 2\beta$), and can be derived to be $\pi - \arcsin \sqrt{1 - \beta^2}$. For the case $\beta = 0.5$, the shock location is

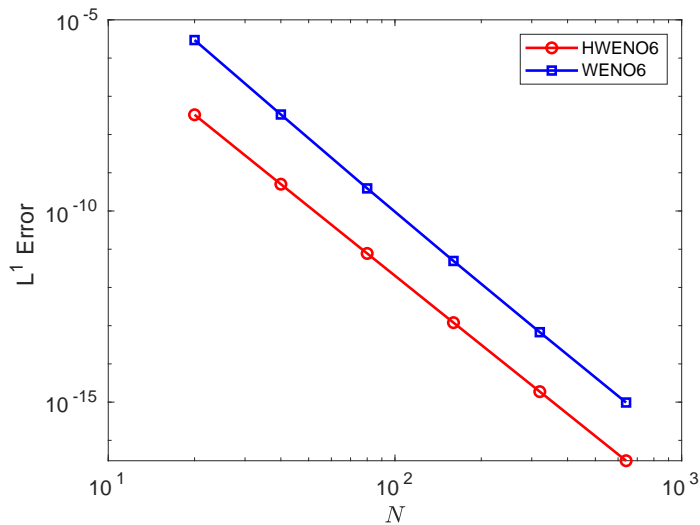


Figure 4.1: L^1 Error for HWENO6 vs. WENO6 for Example 4.1.

approximately 2.0944. The numerical solution on the uniform meshes is shown in the Figure 4.2. We can see that the numerical shock is at the correct location and is resolved well.

Example 4.3. We consider the steady state solutions of the Burgers equation with a different source term, which depends on the solution itself:

$$\left(\frac{u^2}{2}\right)_x = -\pi \cos(\pi x)u, \quad x \in [0, 1] \quad (4.3)$$

equipped with the boundary conditions $u(0) = 1$ and $u(1) = -0.1$. This problem has two steady state solutions with shocks

$$u(x) = \begin{cases} u^+ = 1 - \sin(\pi x) & \text{if } 0 \leq x < x_s, \\ u^- = -0.1 - \sin(\pi x) & \text{if } x_s \leq x \leq 1, \end{cases}$$

where $x_s = 0.1486$ or $x_s = 0.8514$. Both solutions satisfy the Rankine-Hugoniot jump condition and the entropy conditions, but only the one with the shock at 0.1486 is stable for a small perturbation. This problem was studied in [15] as an example of multiple steady states for one-dimensional transonic flows. This case is tested to demonstrate that starting with a reasonable perturbation of the stable steady state, the numerical solution converges to the stable one.

The initial condition is given by

$$u_0(x) = \begin{cases} 1 & \text{if } 0 \leq x < 0.5, \\ -0.1 & \text{if } 0.5 \leq x \leq 1, \end{cases}$$

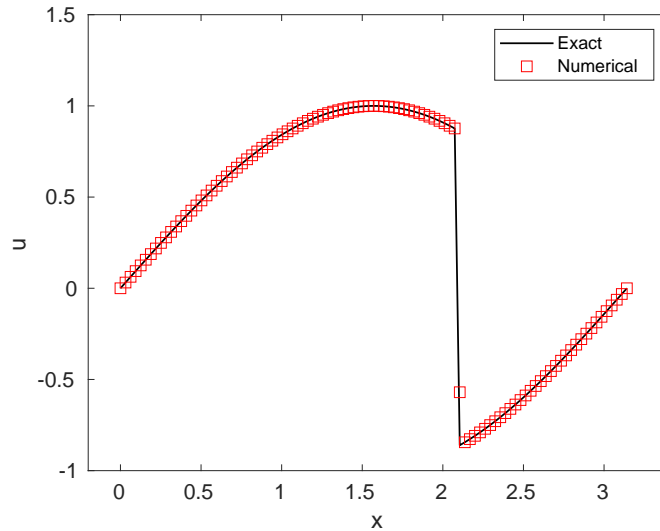


Figure 4.2: The numerical solution (symbols) versus the exact solution (solid line) for the Example 4.2 with 100 cells.

where the initial jump is located in the middle of the position of the shocks in the two admissible steady state solution. The numerical result and the exact solution are displayed in the Figure 4.3. We can see the shock location and good resolution of the shock. And we also obtain the sixth order accuracy of our scheme in a smooth region $[0.5, 1]$ from the Table 4.2. Note that in this case the source term is dependent to the numerical solution.

Table 4.2: Errors and numerical orders of accuracy for the sixth order RD finite difference HWENO scheme for the Example 4.3 at $[0.5, 1]$.

N	L^1 error	Order	L^∞ error	Order
20	5.23E-07		7.28E-07	
40	1.10E-08	5.58	1.50E-08	5.60
80	2.01E-10	5.77	2.78E-10	5.76
160	3.39E-12	5.89	4.78E-12	5.86
320	5.49E-14	5.95	7.85E-14	5.93
640	8.73E-16	5.97	1.26E-15	5.96

Example 4.4. We solve the steady state solutions of the one-dimensional shallow water equation

$$\begin{pmatrix} hu \\ hu^2 + \frac{1}{2}gh^2 \end{pmatrix}_x = \begin{pmatrix} 0 \\ -ghb_x \end{pmatrix}, \quad (4.4)$$

where h denotes the water height, u is the velocity of the fluid, $b(x)$ represents the bottom topography and g is the gravitational constant.

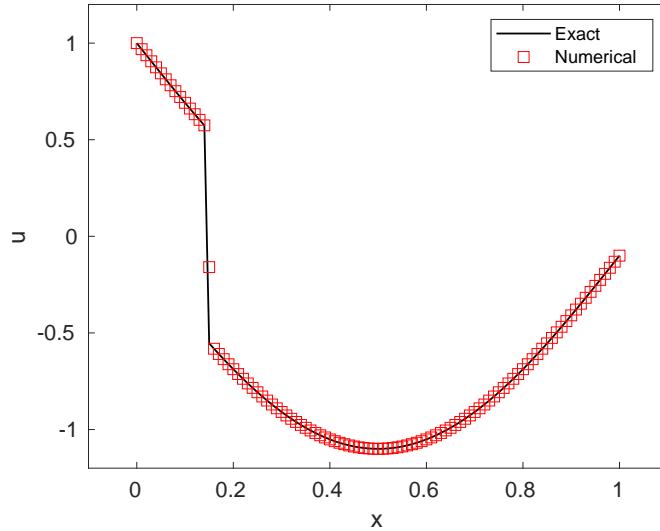


Figure 4.3: The numerical solution (symbols) versus the exact solution (solid line) for the Example 4.3 with 100 cells.

Starting from a stationary initial condition, which itself is a steady state solution, we can check the order of accuracy. The smooth bottom topography is given by

$$b(x) = 5 \exp^{-\frac{2}{5}(x-5)^2}, \quad x \in [0, 10].$$

The initial condition is the stationary solution

$$h + b = 10, \quad hu = 0$$

and the exact steady state solution is imposed as the boundary condition.

We test our scheme on uniform meshes. The numerical accuracies are shown in the Table 4.3. We can clearly see the orders of accuracies and errors. Also, the Figure 4.4 shows that the comparison of L^1 error between HWENO and WENO integration. We can clearly observe that the L^1 error of the sixth order scheme using the HWENO integration is smaller than that of the sixth order scheme using the WENO integration at the same grid.

Example 4.5. We test our scheme on the steady state solution of the one-dimensional nozzle flow problem

$$\begin{pmatrix} \rho u \\ \rho u^2 + p \\ u(E + p) \end{pmatrix}_x = -\frac{A'(x)}{A(x)} \begin{pmatrix} \rho u \\ \rho^2 u^2 / \rho \\ u(E + p) \end{pmatrix}, \quad x \in [0, 1], \quad (4.5)$$

Table 4.3: Errors and numerical orders of accuracy for the water height h of the sixth order RD finite difference HWENO scheme for the Example 4.4.

N	L^1 error	Order	L^∞ error	Order
20	1.02E-04		6.29E-04	
40	1.69E-06	5.91	8.27E-06	6.25
80	2.39E-08	6.14	1.24E-07	6.06
160	3.65E-10	6.03	1.92E-09	6.01
320	5.66E-12	6.01	2.98E-11	6.01
640	8.82E-14	6.00	4.65E-13	6.00

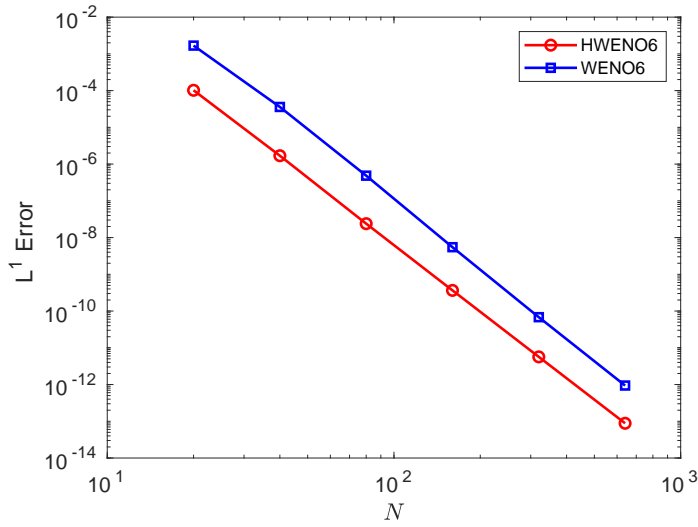


Figure 4.4: L^1 Error for HWENO6 vs. WENO6 for Example 4.4.

where ρ is the density, u is the velocity of the fluid, E is the total energy, $\gamma = 1.4$ is the gas constant, $p = (\gamma - 1)(E - \frac{1}{2}\rho u^2)$ is the pressure and $A(x)$ represents the area of the cross-section of the nozzle.

We start with an isentropic initial condition, with a shock at $x = 0.5$. The density ρ and pressure p at $-\infty$ are 1, and the inlet Mach number at $x = 0$ is 0.8. The outlet Mach number at $x = 1$ is 1.8, with linear Mach number distribution before and after the shock. The area of the cross-section $A(x)$ is then determined by the relation

$$A(x)f(\text{Mach number at } x) = \text{constant}, \quad \forall x \in [0, 1],$$

where

$$f(w) = \frac{w}{(1 + \delta_0 w^2)^{p_0}}, \quad \delta_0 = \frac{1}{2}(\gamma - 1), \quad p_0 = \frac{1}{2} \cdot \frac{\gamma + 1}{\gamma - 1}.$$

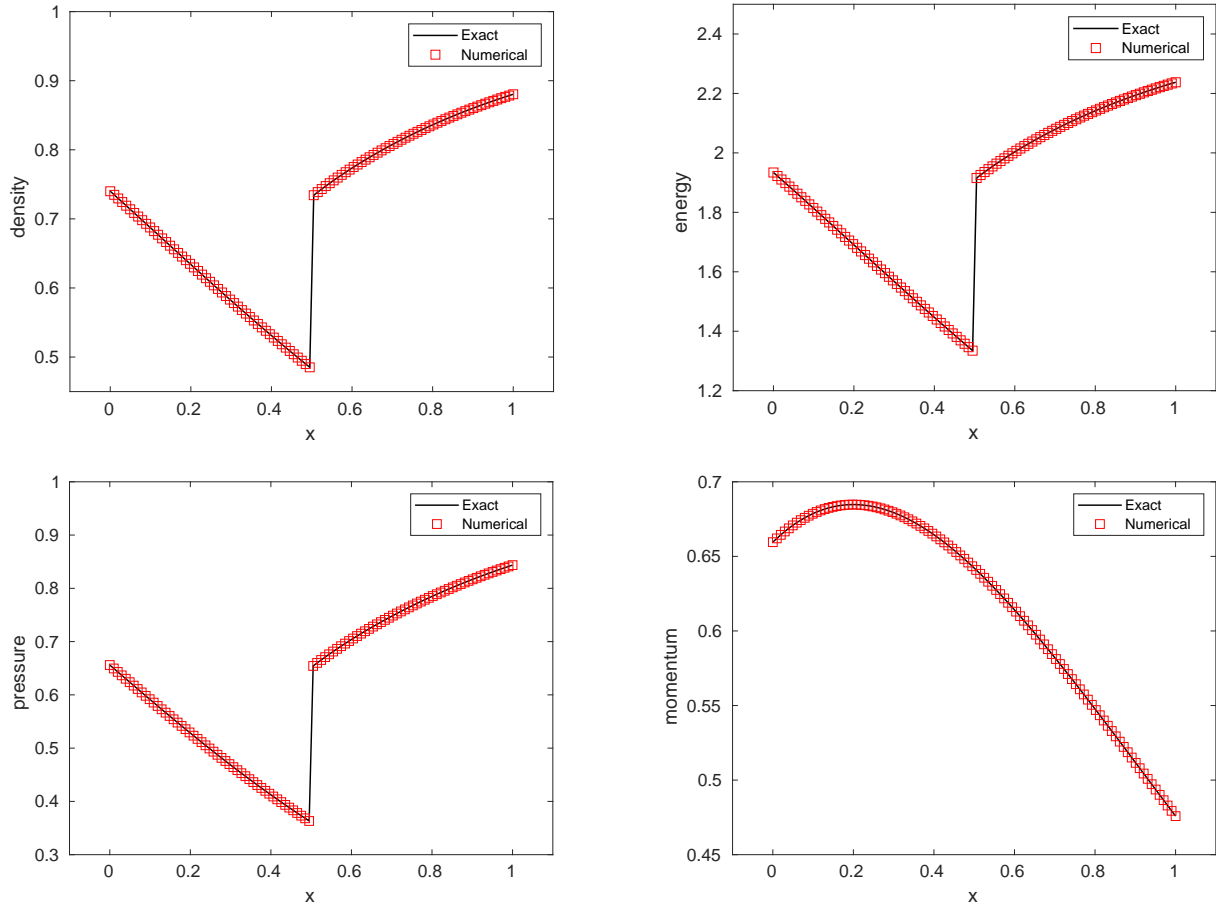


Figure 4.5: Nozzle flow problem with 101 cells. Solid lines: exact solution; symbols: numerical solution. Top left: density; top right: total energy; bottom left: pressure; bottom right: momentum.

From the Figure 4.5, we can clearly see that the shock is resolved well. In comparison with the sixth RD finite difference WENO method, it is faster to convergence to the steady state, see Figure 4.6.

4.2 The two-dimensional problems

Example 4.6. We solve the steady state problem of two-dimensional Burgers equation with a source term

$$\left(\frac{1}{\sqrt{2}}\frac{u^2}{2}\right)_x + \left(\frac{1}{\sqrt{2}}\frac{u^2}{2}\right)_y = \sin\left(\frac{x+y}{\sqrt{2}}\right)\cos\left(\frac{x+y}{\sqrt{2}}\right), \quad (4.6)$$

where $(x, y) \in \left[0, \frac{\pi}{\sqrt{2}}\right] \times \left[0, \frac{\pi}{\sqrt{2}}\right]$ with the initial condition given by

$$u_0(x, y) = \beta \sin\left(\frac{x+y}{\sqrt{2}}\right). \quad (4.7)$$

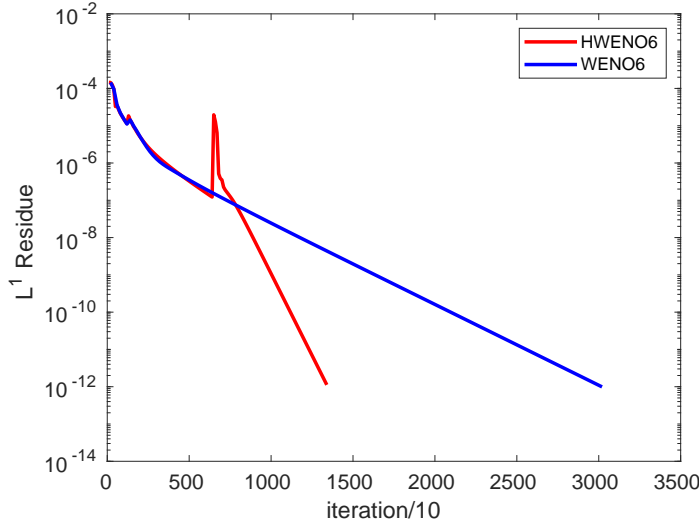


Figure 4.6: The convergence history of L^1 residue for Nozzle flow problem.

This is the one-dimensional problem studied in the Example 4.1 along the northeast-southwest diagonal. Since our grids are not aligned with the diagonal, this is a truly two-dimensional test case. Here we take the boundary conditions to be the exact solution of the steady state problem.

For this example, we take $\beta = 1.2$, which gives a smooth steady state solution $u(x, y) = \sin\left(\frac{x+y}{\sqrt{2}}\right)$. The errors and numerical orders are shown in the Table 4.4. It can be clearly seen that the the sixth order accuracy is achieved in the L^1 error case.

Table 4.4: Errors and numerical orders of accuracy for the sixth order RD finite difference HWENO scheme for the Example 4.6 with $N \times N$ cells.

$N \times N$	L^1 error	Order	L^2 error	Order	L^∞ error	Order
10×10	2.93E-07		4.61E-07		2.00E-06	
20×20	4.13E-09	6.15	7.69E-09	5.90	6.38E-08	4.97
40×40	6.19E-11	6.06	1.32E-10	5.86	2.00E-09	4.99
80×80	9.45E-13	6.03	2.29E-12	5.85	6.27E-11	5.00
160×160	1.44E-14	6.03	3.98E-14	5.85	1.96E-12	5.00

Example 4.7. We consider the steady state solution of the following problem:

$$\left(\frac{1}{\sqrt{2}} \frac{u^2}{2}\right)_x + \left(\frac{1}{\sqrt{2}} \frac{u^2}{2}\right)_y = -\pi \cos\left(\pi \frac{x+y}{\sqrt{2}}\right)u, \quad (4.8)$$

where $(x, y) \in \left[0, \frac{1}{\sqrt{2}}\right] \times \left[0, \frac{1}{\sqrt{2}}\right]$. This is the one-dimensional problem in the Example 4.2 along the northeast-southwest diagonal line. Inflow boundary conditions are given by the exact solution

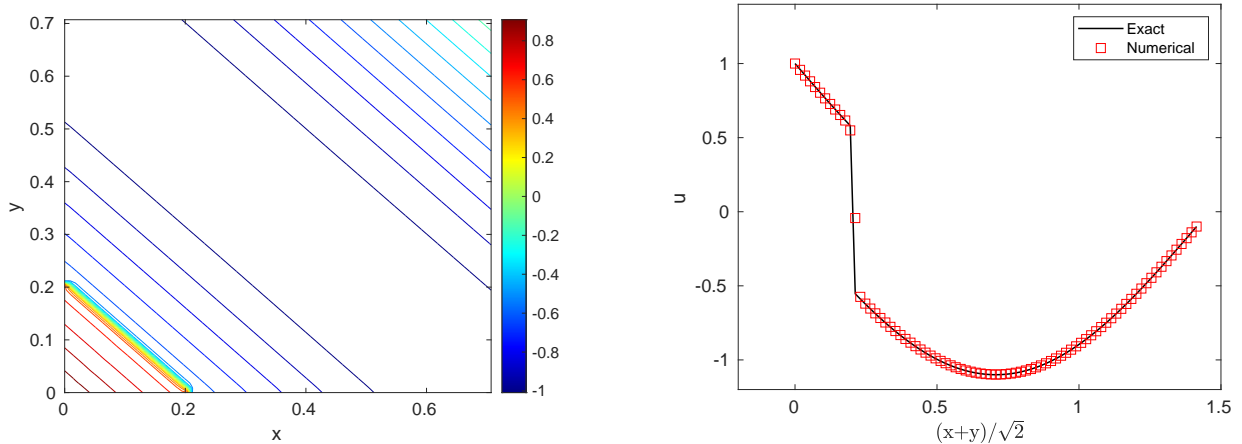


Figure 4.7: Example 4.7 with 80×80 cells. Left: 25 equally spaced contours of the solution from -1.2 to 1.1; right: the numerical solution (symbols) versus the exact solution (solid line) along the cross-section through the northeast to southwest diagonal.

of the steady state problem. Again, since our grids are not aligned with the diagonal line, this is a truly two-dimensional test case. As before, this problem has two steady state solutions with shocks

$$u(x, y) = \begin{cases} 1 - \sin\left(\pi \frac{x+y}{\sqrt{2}}\right) & \text{if } 0 \leq \frac{x+y}{\sqrt{2}} < x_s, \\ -0.1 - \sin\left(\pi \frac{x+y}{\sqrt{2}}\right) & \text{if } x_s \leq \frac{x+y}{\sqrt{2}} \leq 1, \end{cases}$$

where $x_s = 0.1486$ or $x_s = 0.8514$. Both solutions satisfy the Rankine-Hugoniot jump condition and the entropy conditions, but only the one with the shock at $\frac{x+y}{\sqrt{2}} = 0.1486$ is stable for a small perturbation.

The initial condition is given by

$$u_0(x, y) = \begin{cases} 1 & \text{if } 0 \leq \frac{x+y}{\sqrt{2}} < 0.5, \\ -0.1 & \text{if } 0.5 \leq \frac{x+y}{\sqrt{2}} \leq 1, \end{cases}$$

where the initial jump is located in the middle of the positions of the shocks in the two admissible steady state solutions. From Figure 4.7, we can see the correct shock location and a good resolution of the solution. The coefficient σ for the dissipation (3.4) is taken as 5.

Example 4.8. We consider the one-dimensional Burgers equation viewed as a two-dimensional steady state problem

$$\left(\frac{u^2}{2}\right)_x + u_y = 0, \quad (x, y) \in [0, 1] \times [0, 1] \quad (4.9)$$

with the boundary conditions

$$u(x, 0) = 1.5 - 2x, \quad u(0, y) = 1.5, \quad u(1, y) = -0.5.$$

The exact solution consists in a fan that merges into a shock which foot is located at $(x, y) = (\frac{3}{4}, \frac{1}{2})$. More precisely, the exact solution is

$$u(x, y) = \begin{cases} \text{if } y \geq 0.5 & \begin{cases} -0.5 & \text{if } -2(x - 3/4) + (y - 1/2) \leq 0, \\ 1.5 & \text{else,} \end{cases} \\ \text{else} & \max\left(-0.5, \min\left(1.5, \frac{x-3/4}{y-1/2}\right)\right). \end{cases}$$

This problem was studied in [10] as a prototype example for shock boundary layer interaction. The initial condition is taken to be $u_0(x, y) = u_0(x, 0) = 1.5 - 2x$. The isolines of the numerical solution and the cross-sections for $y = 0.25$ across the fan, for $y = 0.5$ right at the junction where the fan becomes a single shock, and at $y = 0.75$ across the shock, are displayed in the Figure 4.8. We can clearly observe good resolution of the numerical scheme for this example. The coefficient σ for the dissipation (3.4) is taken as 2.

Example 4.9. We consider a Cauchy-Riemann problem

$$\frac{\partial W}{\partial t} + A \frac{\partial W}{\partial x} + B \frac{\partial W}{\partial y} = 0, \quad (x, y) \in [-2, 2] \times [-2, 2], \quad t > 0, \quad (4.10)$$

where

$$A = \begin{pmatrix} 1 & 0 \\ 0 & -1 \end{pmatrix} \quad \text{and} \quad B = \begin{pmatrix} 0 & 1 \\ 1 & 0 \end{pmatrix} \quad (4.11)$$

with the following Riemann data $W = (u, v)^T$:

$$u = \begin{cases} 1 & \text{if } x > 0 \text{ and } y > 0 \\ -1 & \text{if } x < 0 \text{ and } y > 0 \\ -1 & \text{if } x < 0 \text{ and } y < 0 \\ 1 & \text{if } x > 0 \text{ and } y < 0 \end{cases} \quad \text{and} \quad v = \begin{cases} 1 & \text{if } x > 0 \text{ and } y > 0 \\ -1 & \text{if } x < 0 \text{ and } y > 0 \\ -1 & \text{if } x > 0 \text{ and } y < 0 \\ 2 & \text{if } x < 0 \text{ and } y < 0 \end{cases}. \quad (4.12)$$

The solution is self-similar, and therefore $W(x, y, t) = \tilde{W}(\frac{x}{t}, \frac{y}{t})$. Let $\xi = \frac{x}{t}$, $\eta = \frac{y}{t}$, then \tilde{W} satisfies

$$(-\xi I + A) \frac{\partial \tilde{W}}{\partial \xi} + (-\eta I + B) \frac{\partial \tilde{W}}{\partial \eta} = 0, \quad (4.13)$$

which can be written as

$$\frac{\partial}{\partial \xi} [(-\xi I + A) \tilde{W}] + \frac{\partial}{\partial \eta} [(-\eta I + B) \tilde{W}] = -2\tilde{W}. \quad (4.14)$$

When $t = 1$, the problem (4.14) can be regarded as a steady state problem and solved by RD method with boundary conditions set as the exact solution and the same initial condition as in (4.15). The coefficient σ for the dissipation (3.4) is taken as 1 and the parameter δ in (2.13) for

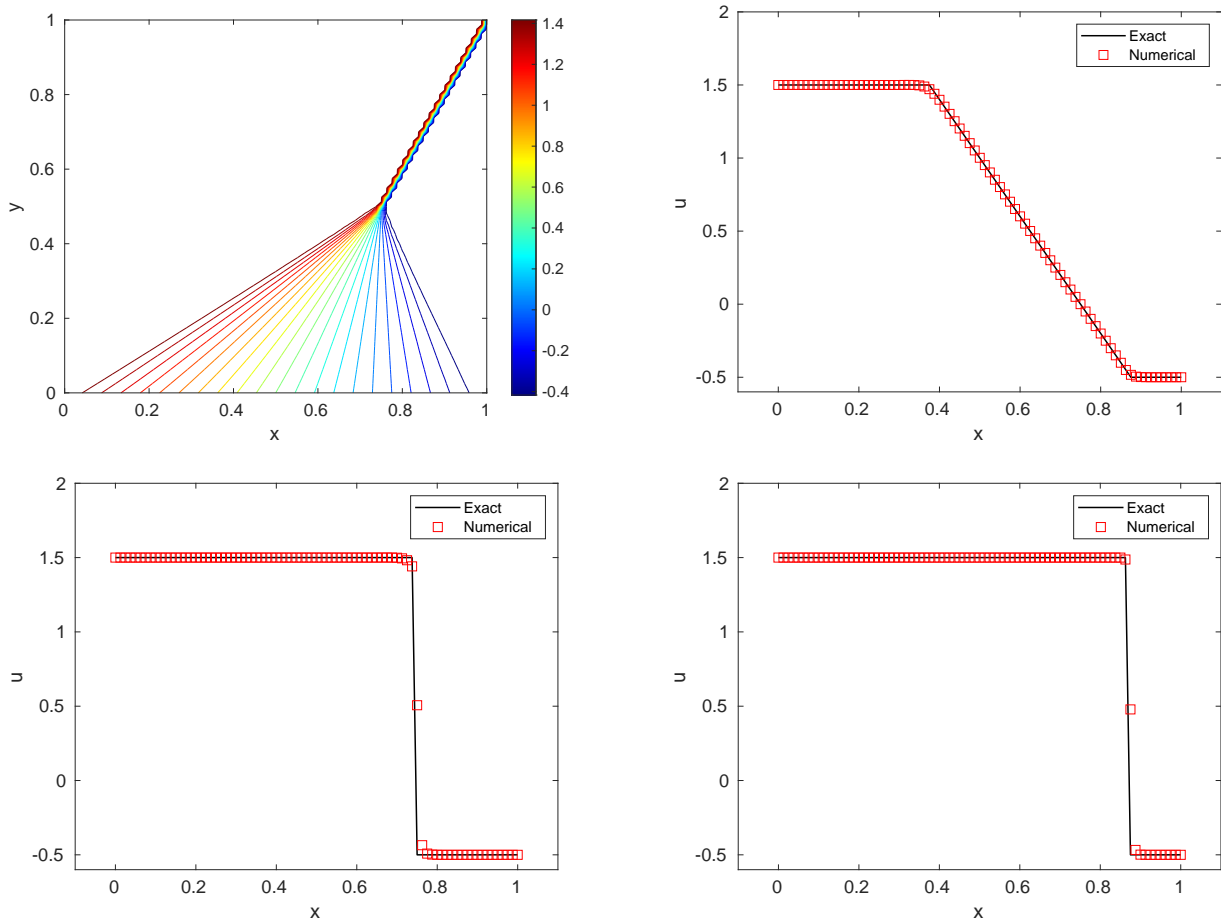


Figure 4.8: Example 4.8 with 80×80 cells. Top left: 25 equally spaced contour lines from -0.6 to 1.6; Top right: cross section at $y = 0.25$; bottom left: cross section at $y = 0.5$; bottom right: cross section at $y = 0.75$. For the cross section, the solid lines are for the exact solution and symbols are for the numerical solution.

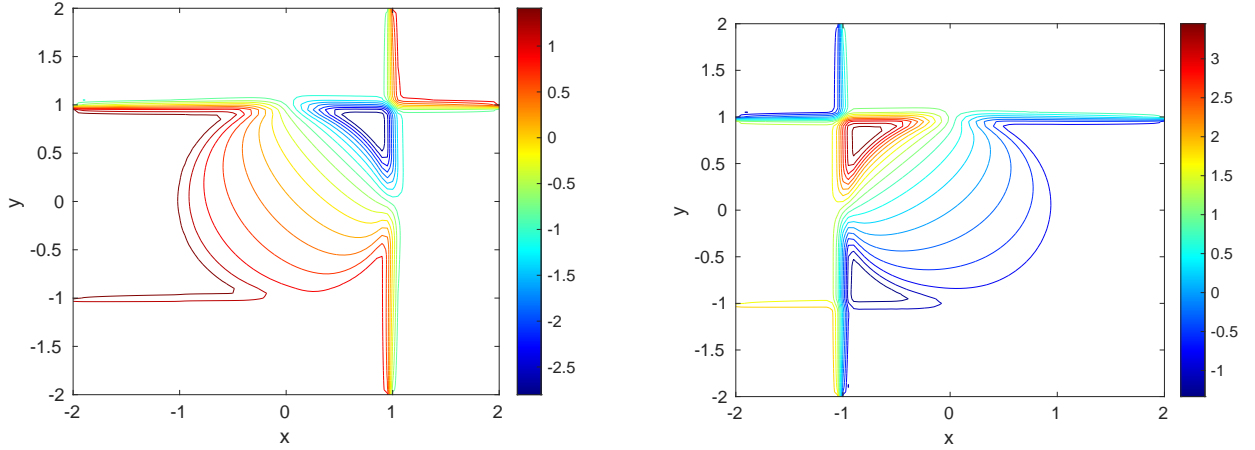


Figure 4.9: Example 4.9 with 80×80 cells. Left: 20 equally spaced contours for u from -3.05 to 1.66; right: 20 equally spaced contour for v from -1.6 to 3.45.

the Roe's entropy correction is taken as 0.4. The numerical results are shown in the Figure 4.9 and the convergence history of L^1 residue is shown in the Figure 4.10.

$$u = \begin{cases} 1 & \text{if } x > 1 \text{ and } y > 1 \\ -1 & \text{if } x > 1 \text{ and } y < 1 \\ -1 & \text{if } x < 1 \text{ and } y > 1 \\ 1.5 & \text{if } x < 1 \text{ and } -1 < y < 1 \\ 1 & \text{if } x < 1 \text{ and } y < -1 \end{cases} \quad \text{and} \quad v = \begin{cases} 1 & \text{if } x > -1 \text{ and } y > 1 \\ -1 & \text{if } x < -1 \text{ and } y > 1 \\ -1 & \text{if } x > -1 \text{ and } y < 1 \\ 1.5 & \text{if } x < -1 \text{ and } -1 < y < 1 \\ 2 & \text{if } x < -1 \text{ and } y < -1 \end{cases}. \quad (4.15)$$

Example 4.10. We consider a regular shock reflection problem of the steady state solution of the two-dimensional Euler equations

$$\mathbf{f}(\mathbf{u})_x + \mathbf{g}(\mathbf{u})_y = 0, \quad (x, y) \in [0, 4] \times [0, 1], \quad (4.16)$$

where $\mathbf{u} = (\rho, \rho u, \rho v, E)^T$, $\mathbf{f}(\mathbf{u}) = (\rho u, \rho u^2 + p, \rho u v, u(E + p))^T$, and $\mathbf{g}(\mathbf{u}) = (\rho v, \rho u v, \rho v^2 + p, v(E + p))^T$. Here ρ is the density, (u, v) is the velocity, E is the total energy and $p = (\gamma - 1)(E - \frac{1}{2}(\rho u^2 + \rho v^2))$ is the pressure. γ is the gas constant which is again taken as 1.4 in our numerical tests.

The initial condition is taken to be

$$(\rho, u, v, p) = \begin{cases} (1.69997, 2.61934, -0.50632, 1.52819) & \text{on } y = 1, \\ (1, 2.9, 0, \frac{1}{\gamma}) & \text{otherwise.} \end{cases}$$

The boundary conditions are given by

$$(\rho, u, v, p) = (1.69997, 2.61934, -0.50632, 1.52819) \quad \text{on } y = 1$$

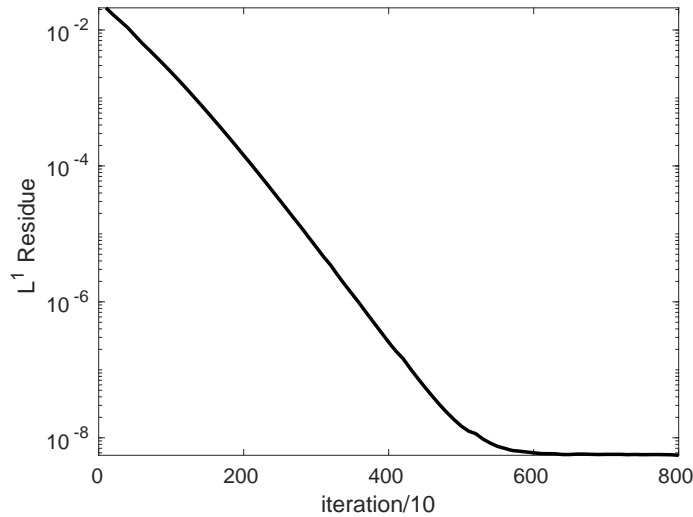


Figure 4.10: The convergence history of L^1 residue for the Cauchy Riemann problem.

and reflective boundary condition on $y = 0$. The left boundary at $x = 0$ is set as inflow with $(\rho, u, v, p) = (1, 2.9, 0, \frac{1}{\gamma})$, and the right boundary at $x = 4$ is set to be an outflow with no boundary conditions prescribed. The numerical results are shown in the Figure 4.11. We can clearly see the good resolutions of the incident and reflected shocks. The coefficient σ for the dissipation (3.4) is taken as 10. The convergence history of L^1 residue is shown in the Figure 4.12.

5 Conclusion

A high order RD conservative conservative finite difference HWENO method was proposed for solving steady state hyperbolic equations with source terms on uniform meshes. The method is based on HWENO approximations to achieve high order accuracy. The idea of residual distribution is adapted and allows us to obtain high order accuracy for steady state problems. We apply this proposed method to both scalar and system problems including Burgers equation, shallow water equations, nozzle flow problem, Cauchy Riemann problem and Euler equations. In all simulations, we observed that we get the sixth order in smooth regions, respectively, and clearly see high resolutions around a shock. The extension to unsteady problems will be explored in future.

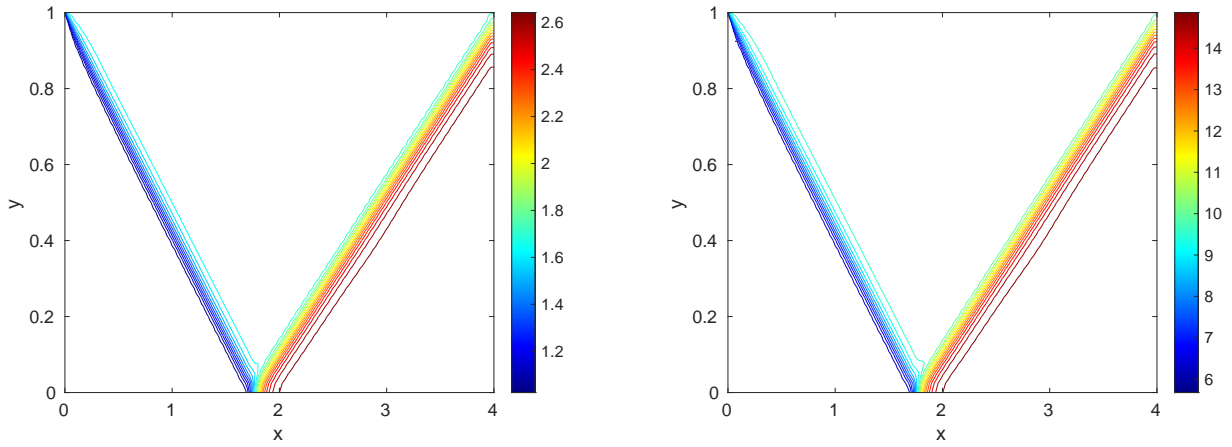


Figure 4.11: Example 4.10 with 160×40 cells. Left: 25 equally spaced contours for the density from 0.87 to 2.72; right: 25 equally spaced contour for the energy from 4.8 to 15.3.

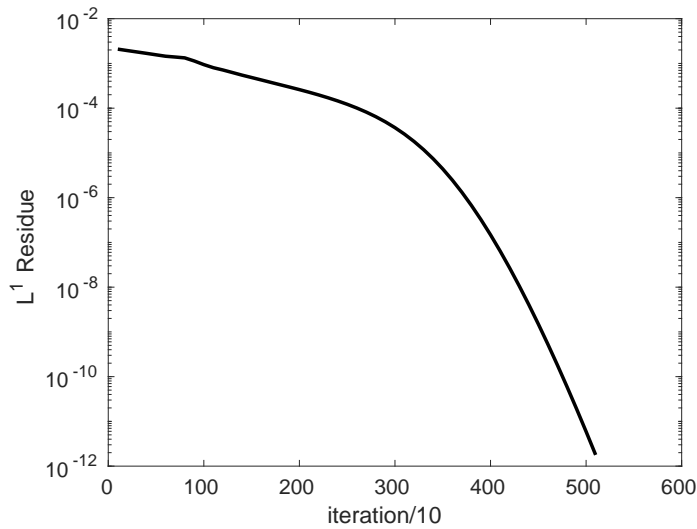


Figure 4.12: The convergence history of L^1 residue for the shock reflection problem.

Acknowledgments

The research was started in 2016 when J. Lin was a visiting Ph.D. student at University of Zürich in Switzerland and she was also partly supported by SNF FZEB-0-166980 grant and National Science Foundation (China) grant 12071392. And thank Professor Xinghui Zhong at Zhejiang University for her valuable comments on the paper.

References

- [1] R. Abgrall. Toward the ultimate conservative scheme: following the quest. *J. Comput. Phys.*, 167(2):277–315, 2001.
- [2] R. Abgrall. High order schemes for hyperbolic problems using globally continuous approximation and avoiding mass matrices. *J. Sci. Comput.*, 73(2-3):461–494, 2017.
- [3] R. Abgrall, P. Bacigaluppi, and S. Tokareva. How to avoid mass matrix for linear hyperbolic problems. In *Numerical mathematics and advanced applications—ENUMATH 2015*, volume 112 of *Lect. Notes Comput. Sci. Eng.*, pages 75–86. Springer, [Cham], 2016.
- [4] R. Abgrall and F. Marpeau. Residual distribution scheme on quadrilateral meshes. *J. Sci. Comput.*, 30(1):131–175, 2007.
- [5] R. Abgrall, K. Mer, and B. Nkonga. A Lax-Wendroff type theorem for residual schemes. In *Innovative methods for numerical solutions of partial differential equations (Arcachon, 1998)*, pages 243–266. World Sci. Publ., River Edge, NJ, 2002.
- [6] R. Abgrall and M. Mezone. Construction of second order accurate monotone and stable residual distribution schemes for unsteady flow problems. *J. Comput. Phys.*, 188(1):16–55, 2003.
- [7] R. Abgrall and M. Mezone. Construction of second-order accurate monotone and stable residual distribution schemes for steady problems. *J. Comput. Phys.*, 195(2):474–507, 2004.
- [8] R. Abgrall and P. L. Roe. High order fluctuation schemes on triangular meshes. *J. Sci. Comput.*, 19(1-3):3–36, 2003. Special issue in honor of the sixtieth birthday of Stanley Osher.

- [9] D. S. Balsara, T. Rumpf, M. Dumbser, and C.-D. Munz. Efficient, high accuracy ADER-WENO schemes for hydrodynamics and divergence-free magnetohydrodynamics. *J. Comput. Phys.*, 228(7):2480–2516, 2009.
- [10] W. Cai, D. Gottlieb, and C.-W. Shu. Essentially nonoscillatory spectral Fourier methods for shock wave calculations. *Math. Comp.*, 52(186):389–410, 1989.
- [11] C.-S. Chou and C.-W. Shu. High order residual distribution conservative finite difference WENO schemes for steady state problems on non-smooth meshes. *J. Comput. Phys.*, 214(2):698–724, 2006.
- [12] C.-S. Chou and C.-W. Shu. High order residual distribution conservative finite difference WENO schemes for convection-diffusion steady state problems on non-smooth meshes. *J. Comput. Phys.*, 224(2):992–1020, 2007.
- [13] A. Csík and H. Deconinck. Space-time residual distribution schemes for hyperbolic conservation laws on unstructured linear finite elements. volume 40, pages 573–581. 2002. ICFD Conference on Numerical Methods for Fluid Dynamics, Part II (Oxford, 2001).
- [14] H. Deconinck, R. Struijs, G. Bourgeois, and P. Roe. Compact advection schemes on unstructured meshes. *Computational Fluid Dynamics*, pages VKI Lecture Series 1993–04, 1993.
- [15] P. Embid, J. Goodman, and A. Majda. Multiple steady states for 1-D transonic flow. *SIAM J. Sci. Statist. Comput.*, 5(1):21–41, 1984.
- [16] A. Harten. High resolution schemes for hyperbolic conservation laws. *J. Comput. Phys.*, 49(3):357–393, 1983.
- [17] G.-S. Jiang and C.-W. Shu. Efficient implementation of weighted ENO schemes. *J. Comput. Phys.*, 126(1):202–228, 1996.
- [18] H. Liu and J. Qiu. Finite difference hermite weno schemes for hyperbolic conservation laws. *J. Sci. Comput.*, 63(2):548–572, 2015.
- [19] H. Paillere, H. Deconinck, and P. Roe. *Conservative upwind residual-distribution schemes based on the steady characteristics of the Euler equations.*

- [20] J. Qiu and C.-W. Shu. Hermite weno schemes and their application as limiters for runge–kutta discontinuous galerkin method: one-dimensional case. *J. Comput. Phys.*, 193(1):115–135, 2004.
- [21] J. Qiu and C.-W. Shu. Hermite weno schemes and their application as limiters for runge–kutta discontinuous galerkin method ii: Two dimensional case. *Comput. Fluids*, 34(6):642–663, 2005.
- [22] J. Qiu and C.-W. Shu. Hermite weno schemes for hamilton–jacobi equations. *J. Comput. Phys.*, 204(1):82–99, 2005.
- [23] Y. Ren, Y. Xing, and J. Qiu. High order finite difference hermite weno fast sweeping methods for static hamilton-jacobi equations, 2020.
- [24] Y. Ren, Y. Xing, D. Wang, and J. Qiu. High order asymptotic preserving hermite weno fast sweeping method for the steady-state sn transport equation.
- [25] P. L. Roe. Approximate Riemann solvers, parameter vectors, and difference schemes. *J. Comput. Phys.*, 43(2):357–372, 1981.
- [26] P. L. Roe and D. Sidilkover. Optimum positive linear schemes for advection in two and three dimensions. *SIAM J. Numer. Anal.*, 29(6):1542–1568, 1992.
- [27] M. D. Salas, S. Abarbanel, and D. Gottlieb. Multiple steady states for characteristic initial value problems. *Appl. Numer. Math.*, 2(3-5):193–210, 1986.
- [28] C.-W. Shu. High order weighted essentially nonoscillatory schemes for convection dominated problems. *SIAM Rev.*, 51(1):82–126, 2009.
- [29] C.-W. Shu and S. Osher. Efficient implementation of essentially nonoscillatory shock-capturing schemes. *J. Comput. Phys.*, 77(2):439–471, 1988.
- [30] C.-W. Shu and S. Osher. Efficient implementation of essentially nonoscillatory shock-capturing schemes. *J. Comput. Phys.*, 77(2):439–471, 1988.
- [31] R. Struijs, H. Deconinck, and P. Roe. Fluctuation splitting for the 2d euler equations. *Computational Fluid Dynamics*, -1, 01 1991.
- [32] Z. Tao, F. Li, and J. Qiu. High-order central hermite weno schemes on staggered meshes for hyperbolic conservation laws. *J. Comput. Phys.*, 281:148–176, 2015.

- [33] Y. H. Zahran and A. H. Abdalla. Seventh order hermite weno scheme for hyperbolic conservation laws. *Comput. Fluids*, 131:66–80, 2016.
- [34] Z. Zhao, Y. Chen, and J. Qiu. A hybrid hermite weno scheme for hyperbolic conservation laws. *J. Comput. Phys.*, 405:109175, 2020.
- [35] Z. Zhao, Y.-T. Zhang, and J. Qiu. A modified fifth order finite difference Hermite WENO scheme for hyperbolic conservation laws. *J. Sci. Comput.*, 85(2):Paper No. 29, 22, 2020.
- [36] J. Zhu and J. Qiu. New finite volume weighted essentially nonoscillatory schemes on triangular meshes. *SIAM J. Sci. Comput.*, 40(2):A903–A928, 2018.